Direct assessment of the acidity of individual surface hydroxyls

https://doi.org/10.1038/s41586-021-03432-3

Received: 2 January 2020

Accepted: 8 March 2021

Published online: 28 April 2021

Check for updates

Margareta Wagner[1,2], Bernd Meyer[3,4], Martin Setvin[1,5], Michael Schmid[1] & Ulrike Diebold[1]✉

The state of deprotonation/protonation of surfaces has far-ranging implications in chemistry, from acid–base catalysis[1] and the electrocatalytic and photocatalytic splitting of water[2], to the behaviour of minerals[3] and biochemistry[4]. An entity's acidity is described by its proton affinity and its acid dissociation constant pK_a (the negative logarithm of the equilibrium constant of the proton transfer reaction in solution). The acidity of individual sites is difficult to assess for solids, compared with molecules. For mineral surfaces, the acidity is estimated by semi-empirical concepts, such as bond-order valence sums[5], and increasingly modelled with first-principles molecular dynamics simulations[6,7]. At present, such predictions cannot be tested—experimental measures, such as the point of zero charge[8], integrate over the whole surface or, in some cases, individual crystal facets[9]. Here we assess the acidity of individual hydroxyl groups on In_2O_3(111)—a model oxide with four different types of surface oxygen atom. We probe the strength of their hydrogen bonds with the tip of a non-contact atomic force microscope and find quantitative agreement with density functional theory calculations. By relating the results to known proton affinities of gas-phase molecules, we determine the proton affinity of the different surface sites of In_2O_3 with atomic precision. Measurements on hydroxylated titanium dioxide and zirconium oxide extend our method to other oxides.

Our work relies on recent developments in high-resolution, non-contact atomic force microscopy (nc-AFM) using the qPlus sensor[10]. Appropriately functionalized tips[11] allow the imaging of the chemical structure of molecules, the evaluation of surface structures[12] and following the diffusion of water clusters in a non-perturbative way[13]. Most importantly, one can probe the properties of individual surface atoms[14], such as their chemical nature[15], their charge[16] or their electronegativity[17].

Here we use a hydroxyl (OH)-functionalized AFM tip for quantitative insights into the acidity of individual surface OH groups. As our AFM measurements are conducted in vacuum, we directly assess the proton affinity (PA)—the key contribution to the acid dissociation constant (pK_a). The PA is defined as the enthalpy change on deprotonating an OH group in the gas phase[18] and the pK_a value is then obtained by adding the Gibbs free energies of solvation (Methods). Although it is difficult to determine absolute PA values, differences can be measured by gas-phase titration with probe molecules with a known PA: in the case of a strong base, by measuring the proton transfer; and for a weak base, where no proton transfer occurs, by measuring adsorption enthalpies[19]. With the AFM tip, we work in the weak basicity limit: its OH group forms a hydrogen bond with a surface OH, and the hydrogen bond strength can be translated into the PA of individual sites.

Our test oxide, In_2O_3(111), offers multiple, well defined surface sites, and has promising applications in catalysis[20,21]. Indium oxide (In_2O_3) crystallizes in the bixbyite structure (space group *Ia*-3) with a cubic unit cell of 10.12 Å. Bulk In atoms are six-fold coordinated (In(6c)) and each O(4c) atom has four bonds of unequal lengths, ranging from 2.12 Å to 2.22 Å (ref. [22]). The (111) surface consists of an O–In–O trilayer and is stable in its bulk-terminated (1 × 1) form (Fig. 1a) with small relaxations[23]. Of the 16 In atoms in the surface unit cell, 4 atoms are In(6c) and 12 atoms are In(5c), that is, they are missing one bond. The 12 O(3c) atoms fall into four categories (α, β, γ and δ)—each type is missing a bond of one particular length. The different coordination of these surface O atoms is reflected in their electronic structure. Figure 1b shows the valence band, which, as is true for most oxides, is mostly of O 2*p* character. The O(γ) are in a strongly relaxed environment and their partial density of states (PDOS) resembles bulk O. The states of the O(β) are highest in energy, and those of O(α) and O(δ) fall in-between. The PDOS peaks at the valence band maximum (VBM) lead to upward shifts of the individual *p*-band centres, indicating increasing reactivity from O(γ) to O(β)[24]; the calculated adsorption energies of an isolated H atom (inset of Fig. 1b) follow such expectations.

We have prepared the (111) surface of an In_2O_3 single crystal in ultrahigh vacuum following established procedures[23]. The sample was imaged at low temperatures with a combined scanning tunnelling microscope (STM) and nc-AFM equipped with a qPlus sensor. The image in Fig. 1c was obtained with an O-terminated tip (prepared by first scanning a titanium dioxide (TiO_2) surface covered with O_2; Extended Data Fig. 1) and shows the shift in resonance frequency during a constant-height scan. The individual O(3c) atoms are clearly

[1]Institute of Applied Physics, TU Wien, Vienna, Austria. [2]Central European Institute of Technology (CEITEC), Brno University of Technology, Brno, Czech Republic. [3]Interdisciplinary Center for Molecular Materials, Friedrich-Alexander-Universität Erlangen-Nürnberg, Erlangen, Germany. [4]Computer Chemistry Center, Friedrich-Alexander-Universität Erlangen-Nürnberg, Erlangen, Germany. [5]Department of Surface and Plasma Science, Faculty of Mathematics and Physics, Charles University, Prague, Czech Republic. ✉e-mail: diebold@iap.tuwien.ac.at

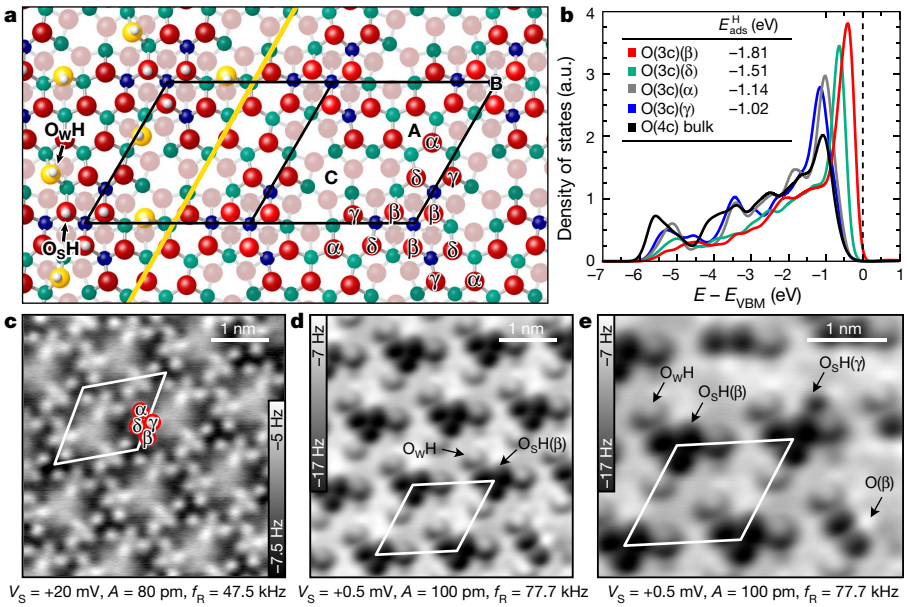

Fig. 1 | The clean and hydroxylated In_2O_3(111) surface. a, Structural model of the relaxed (1 × 1) surface with the positions of three-fold symmetry axes labelled A, B and C. Each surface unit cell contains four six-fold coordinated In(6c) atoms (blue), 12 In(5c) atoms (green), 12 O(3c) atoms (red) and 12 O(4c) atoms below (shaded red). The four types of O(3c) atom are labelled α, β, γ and δ. At saturation, left of the yellow line, three water molecules adsorb dissociatively at equivalent sites, each forming an O_WH hydroxyl and a surface hydroxyl O_SH by protonating an O(β). **b**, PDOS of the various O(3c) atoms, plotted with respect to the VBM. The calculated adsorption energies E_{ads} of H atoms for each of the O(3c) are listed in the inset. **c**, Constant-height nc-AFM image taken with an O-terminated tip in repulsion. **d**, Non-contact AFM image of the surface saturated by exposure to water vapour at room temperature. The O_WH and O_SH(β) sit at the positions indicated in **a**, and are clearly distinguished by their frequency shift. **e**, Surface after a proton was transferred from an O(β) site to an O(γ) site by manipulation with the tip. Imaging parameters for **c**–**e** are shown at the bottom of each frame: sample bias voltage V_S, oscillation amplitude A and resonance frequency of the qPlus sensor f_R. a.u., arbitrary units.

distinguished. Representative AFM images with an OH-terminated tip show the surface In atoms instead (Extended Data Figs. 1, 2).

To hydroxylate the surface, the sample was exposed to water vapour at room temperature. Water adsorbs dissociatively[25] with a saturation coverage of three molecules per unit cell. Only the area near site 'B' (Fig. 1a) is active for adsorption: the hydroxyl stemming from the water molecule (O_WH) always bridges two In(5c), and the split-off proton forms a surface hydroxyl (O_SH) at the neighbouring O(β) (left side of Fig. 1a). This results in a 'propeller type' configuration of three equivalent O_WH–O_SH(β) pairs (see the AFM image in Fig. 1d). The precise location of these hydroxyls was discerned from images taken with different water coverages and tip–sample distances (Extended Data Figs. 3, 4). Dissociative adsorption of three molecules per unit cell leads to only small changes in the electronic structure and the reactivity of the unprotonated surface sites (Extended Data Fig. 8).

To construct hydroxyls at other surface O(3c) sites, we resorted to manipulations with the STM tip (Extended Data Fig. 5). Voltage pulsing and/or scanning with more than +3.5 V desorbs protons from the O_SH (ref. [25]) and these can re-adsorb on an O(3c) close to the original O_SH(β). We could create O_SH(γ) (as in Fig. 1e) and O_SH(δ), but the O(α) are located farther from the site where the water adsorbs, and formation of an O_SH(α) was observed only once during our experiments. Figure 2a shows short-range force–distance curves ($F(z)$) taken on the various hydroxyls. These measurements were robust and reproducible; several datasets are shown. The z at the $F(z)$ minima reflect the vertical positions of the hydroxyls (see also Fig. 3). The force minima show a clear trend: the stronger the H atom is bound to a surface O atom (compare Fig. 1b), the shallower the minimum.

The $F(z)$ curves were calculated from first principles using density functional theory (DFT; Fig. 2b). Several tip models were tried. A tip composed of In_2O_3 and terminated with an OH group proved to be stable and inert when bringing it close to the surface (Fig. 2c, Extended Data Fig. 9). It is reasonable to assume that an STM/AFM tip is coated with the same material as the sample under investigation[26]: the material is transferred during 'tip preparation' procedures such as voltage pulses. In fact, it is difficult to avoid this happening. When scanning water-exposed oxide surfaces, an OH-terminated tip was reported to be the most stable and common termination, and the magnitude of the forces in Fig. 2 is comparable to previous nc-AFM measurements on TiO_2 with OH-terminated tips[26,27]. The quantitative agreement between the measured and calculated $F(z)$ curves in Fig. 2 is a strong indication that the calculated structure correctly reproduces the properties of the tip used in experiment.

Note that the $F(z)$ curves were taken in the attractive regime, that is, negative values of F imply that the tip experiences a stronger attraction to the surface. Figure 2c illustrates what happens. During the approach, a hydrogen bond forms between the O at the tip and the proton of the surface hydroxyl. Integrating the $F(z)$ curves gives the interaction potential $E(z)$; the more attractive $F(z)$, the deeper the energy minimum of $E(z)$. Typically, the minima of $F(z)$ and $E(z)$ show a linear correlation[28] (Extended Data Fig. 11b); thus, the force minimum of the $F(z)$ curves is a direct measure of the strength of the hydrogen bond between the tip and the surface OH.

Figure 3a evaluates how the hydroxyls interact with the tip. In the absence of the tip, the O–H bond lengths of the various hydroxyls on In_2O_3 show only small variations. Under the influence of the tip, the more weakly bonded proton on the O(γ) experiences a substantial displacement Δ, whereas the proton on the O_W hardly changes its position. Figure 3c shows the correlation between the force minimum and the length of the hydrogen bond between the tip and the surface hydroxyl (evaluated at the energy minimum, that is, at $F(z) = 0$): A surface hydroxyl will form weak hydrogen bonds to the tip if the covalent bond within the hydroxyl is strong (that is, the surface O has a high PA, such as the O_W). Conversely, weakly bound protons (located at surface Os

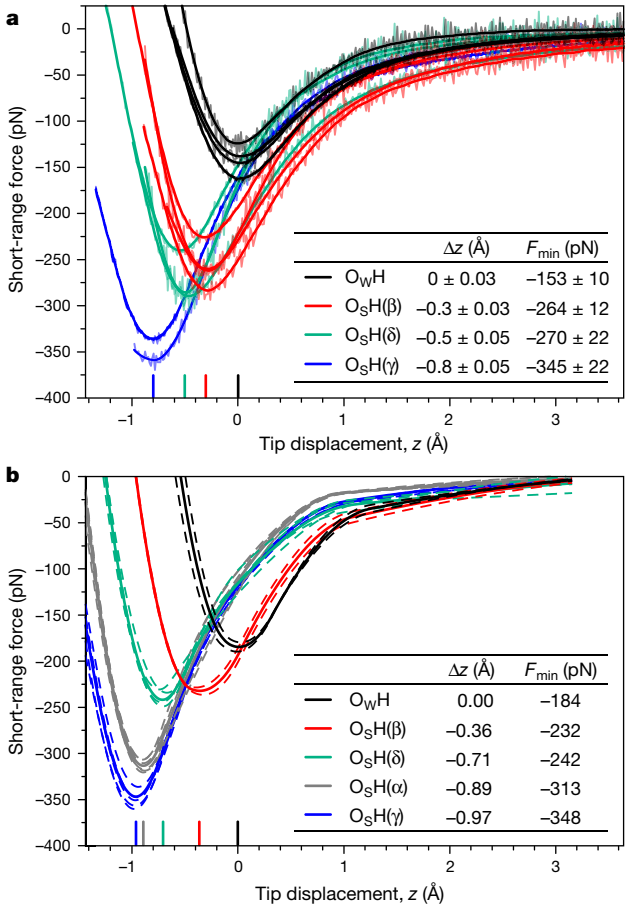

Fig. 2 | Probing individual surface hydroxyls with the AFM tip. a, Experimental short-range force–distance curves, $F(z)$, for the OH groups initially formed on water dissociation, O_WH and $O_SH(\beta)$, as well as for $O_SH(\delta)$ and $O_SH(\gamma)$ that were constructed by manipulation with the tip. Results from four independent datasets are shown. The tip displacement z is given with respect to the position of the O_WH force curve minimum ($z = 0$). The postitions of the minima are indicated on the z axis for all OH groups by short coloured lines; the calculated geometric heights of the O atoms in absence of the tip are listed in Fig. 3a. The errors for the force minimum (F_{min}) and displacement (Δz) provided in the inset were derived using Student's t-distribution with a confidence interval equivalent to 1σ (68.27%). **b**, Calculated short-range force–distance curves. Dashed curves are individual calculations for different tip orientations and sites in the unit cell (see Methods) and solid lines are the averaged curves. **c**, Tip–sample configuration for various separations while probing an $O_SH(\beta)$ group. O_W, yellow; H, white; O(3c) and O(4c), red; In(6c), blue; In(5c), green. For full videos, see the Supplementary Information.

with a low PA, such as the O(γ)) can form stronger hydrogen bonds to the tip. The O at the tip and the O at the surface compete for the proton, hence the force minima of the $F(z)$ curves serve as a direct measure of the PA of the surface O of the probed OH group. Indeed, the values of the force minima in Figs. 2, 3 follow the reactivity trend expected for the different sites; the tip experiences the highest attractive force from the proton bound to the least reactive surface site (lowest PA and strongest acid, bottom right in Fig. 3c). The hydrogen bond between the tip and the surface becomes progressively weaker (less pronounced force minimum) when going from $O_SH(\gamma)$ to $O_SH(\delta)$ to $O_SH(\beta)$; the O_WH exhibits the smallest interaction with the O atom of the tip (highest PA, weakest acid).

To further test how $F(z)$ measurements relate to PA, and to put our results on a quantitative footing, we performed additional DFT calculations. We chose probe molecules with a wide range of known PAs (Extended Data Fig. 11a). Keeping the same tip model, we calculated $F(z)$ curves on these molecules. In the calculations, the molecules were oriented with their OH group pointing towards the tip, similar to the OH groups on the In_2O_3 surface. The backbone of the molecules was fixed, and only the OH was allowed to relax in response to the approaching tip.

Figure 4 shows the calculated minima of the $F(z)$ curves as function of the PA of the probe molecules (stars): their relationship is almost perfectly linear. With this scaling relation, we derive values for the PAs of the different surface O atoms from the measured $F(z)$ curves (see coloured lines in Fig. 4). To test the reliability of this procedure, we compare the so-derived ΔPAs of the surface sites with ΔPAs calculated with DFT; that is, the change in energy when the proton is moved to various sites (double arrows in Fig. 4). We find good agreement. As expected, the PA of the surface oxygen atoms on In_2O_3 are higher than the PA values assigned to hydroxyls in zeolites[19]; the large spread in PA values could assist dehydrogenation/hydrogenation reactions. The force minima also scale with the pK_a, albeit with larger scatter because of the different solubilities of the molecules (Extended Data Fig. 11c, d).

To validate the transferability of our approach, we applied the same method to hydroxyls on two different surfaces, $TiO_2(110)$ and an ultrathin zirconium oxide film. Each time, the tip was functionalized and characterized on hydroxylated In_2O_3; various O_WH and $O_SH(\beta)$ on

a

	Geometric O height without tip (Å)	Hydrogen bond length (Å) at $F(z) = 0$	Surface O–H bond length (Å) Without tip	With tip at $F(z) = 0$	Δ
O_WH	0	2.013	0.976	0.983	+0.007
$O_SH(\beta)$	−0.308	1.869	0.978	0.991	+0.013
$O_SH(\delta)$	−0.553	1.797	0.979	0.996	+0.017
$O_SH(\alpha)$	−0.689	1.767	0.980	1.001	+0.021
$O_SH(\gamma)$	−0.779	1.697	0.979	1.004	+0.025
O_SH/TiO_2		1.584	0.976	1.013	+0.037

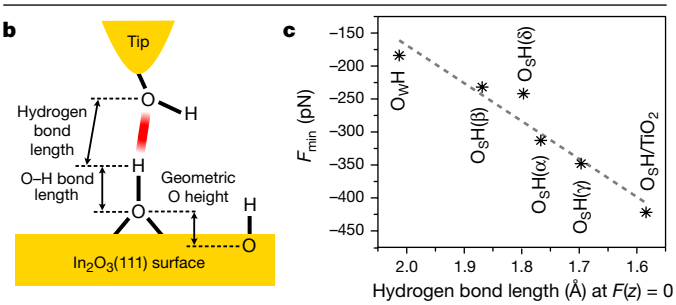

Fig. 3 | Evaluation of theoretical force curves of hydroxyls on $In_2O_3(111)$ and $TiO_2(110)$. a, Oxygen atom heights and various OH bond lengths with and without the tip. **b**, Sketch of the distances shown in **a**. **c**, The length of the hydrogen bond formed between the tip and the surface OH group, evaluated at the energy minimum ($F(z) = 0$), scales with the force minima.

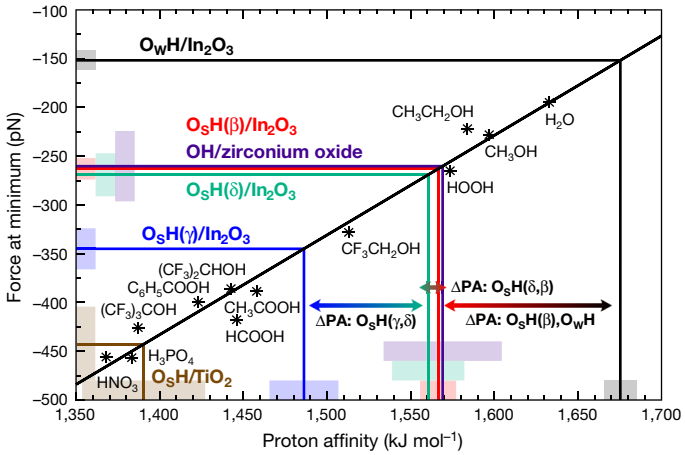

Fig. 4 | Relating AFM-measured force minima to PA using a calibration line. The minima in calculated $F(z)$ curves on various probe molecules (stars), using the tip model shown in Fig. 2c, are related to their gas-phase PAs. The relationship is linear, and the resulting calibration line (black diagonal line) is used to convert experimental force minima to PA. The various hydroxyls on $In_2O_3(111)$ are indicated as $O_SH(\gamma)$ (blue), $O_SH(\delta)$ (green), $O_SH(\beta)$ (red) and O_WH (black). PA differences, ΔPA, calculated after translating protons between various oxygen atoms at $In_2O_3(111)$, are shown by double-headed arrows. Experimentally determined $F(z)$ minima on hydroxyls on $TiO_2(110)$ (brown) and on an ultrathin zirconium oxide film[30] (purple) are also included; here $F(z)$ curves were measured with a comparable tip, functionalized and checked on hydroxylated $In_2O_3(111)$. The coloured shaded bars indicate the respective errors, derived using the Student's t-distribution with a confidence interval equivalent to 1σ (68.27%).

$In_2O_3(111)$ gave the same $F(z)$ as in Fig. 2. Surface hydroxyls on $TiO_2(110)$ have been studied extensively and were prepared on a slightly reduced sample with vacancies in the so-called bridging O_S rows[26]. Water dissociates at room temperature, each O_WH fills a vacancy and a proton is transferred to another bridging O_S, resulting in only one type of O_SH (ref. [26]). The calculated adsorption energy of H (with respect to gas phase H_2) is −0.56 eV (ref. [29]), that is, much weaker than any on In_2O_3. The calculated $F(z)$ (with the hydroxylated InO_x tip) indeed show a lower minimum and a shorter hydrogen bond between the tip and the sample (Fig. 3c). The calculated $F(z)$ values agree well with the experimental values (Extended Data Fig. 7). The PA value obtained from the experimental force minimum for a surface O on $TiO_2(110)$ is much lower than on In_2O_3, as expected for this much more acidic surface with a point of zero charge of 5.8 compared with 8.9 for In_2O_3 (ref. [8]; Fig. 4). In recent decades, many metal oxide systems have been thoroughly characterized with surface science techniques, often in the form of ultrathin films on metal substrates. Figure 4 includes a data point from a representative measurement on ultrathin zirconium oxide prepared by oxidizing a $Pt_3Zr(0001)$ alloy (Extended Data Fig. 7)[30]. The point of zero charge of zirconium dioxide is similar to that of In_2O_3 (ref. [8]), and, indeed, the PA derived from Fig. 4 is in the same range.

Functionalizing tips is common practice in atomically resolved nc-AFM, albeit this is usually done by attaching one molecule[11] to a metallic tip, instead of coating the tip with a specific material as done here. The robustness of the In_2O_3-covered, OH-terminated tip, its high intrinsic PA and the large spread of surface O atoms on $In_2O_3(111)$ that can be used as calibration points suggest that our method can be used as a general tool to measure PAs on an atom-by-atom basis. Our method is not only limited to hydroxyls on perfect surfaces but also applicable for hydroxyls at defects, steps and impurities that can be identified in atomically resolved images.

Online content

Any methods, additional references, Nature Research reporting summaries, source data, extended data, supplementary information, acknowledgements, peer review information; details of author contributions and competing interests; and statements of data and code availability are available at https://doi.org/10.1038/s41586-021-03432-3.

1. Kramer, G. J., van Santen, R. A., Emeis, C. A. & Nowak, A. K. Understanding the acid behaviour of zeolites from theory and experiment. *Nature* **363**, 529–531 (1993).
2. She, Z. W. et al. Combining theory and experiment in electrocatalysis: insights into materials design. *Science* **355**, eaad4998 (2017).
3. Brown, G. E. Jr & Calas, G. Mineral–aqueous solution interfaces and their impact on the environment. *Geochem. Perspect.* **1**, 483–742 (2012).
4. Silverman, R. B. *Organic Chemistry of Enzyme-Catalyzed Reactions* (Academic Press, 2002).
5. Hiemstra, T., Venema, P. & Riemsdijk, W. Intrinsic proton affinity of reactive surface groups of metal (hydr)oxides: the bond valence principle. *J. Colloid Interface Sci.* **184**, 680–692 (1996).
6. Cheng, J. & Sprik, M. Acidity of the aqueous rutile TiO_2(110) surface from density functional theory based molecular dynamics. *J. Chem. Theory Comput.* **6**, 880–889 (2010).
7. Gittus, O. R. von Rudorff, G. F., Rosso, K. M. & Blumberger, J. Acidity constants of the hematite–liquid water interface from ab initio molecular dynamics. *J. Phys. Chem. Lett.* **9**, 5574–5582 (2018).
8. Kosmulski, M. Compilation of PZC and IEP of sparingly soluble metal oxides and hydroxides from literature. *Adv. Colloid Interface Sci.* **152**, 14–25 (2009).
9. Bullard, J. W. & Cima, M. J. Orientation dependence of the isoelectric point of TiO_2 (rutile) surfaces. *Langmuir* **22**, 10264–10271 (2006).
10. Giessibl, F. J. The qPlus sensor, a powerful core for the atomic force microscope. *Rev. Sci. Instrum.* **90**, 011101 (2019).
11. Gross, L., Mohn, F., Moll, N., Liljeroth, P. & Meyer, G. The chemical structure of a molecule resolved by atomic force microscopy. *Science* **325**, 1110–1114 (2009).
12. Setvín, M. et al. Polarity compensation mechanisms on the perovskite surface $KTaO_3$(001). *Science* **359**, 572–575 (2018).
13. Peng, J. et al. The effect of hydration number on the interfacial transport of sodium ions. *Nature* **557**, 701–705 (2018); correction **563**, E18 (2018).
14. Lantz, M. A. et al. Quantitative measurement of short-range chemical bonding forces. *Science* **291**, 2580–2583 (2001).
15. Sugimoto, Y. et al. Chemical identification of individual surface atoms by atomic force microscopy. *Nature* **446**, 64–67 (2007).
16. Gross, L. et al. Measuring the charge state of an adatom with noncontact atomic force microscopy. *Science* **324**, 1428–1431 (2009).
17. Onoda, J., Ondráček, M., Jelínek, P. & Sugimoto, Y. Electronegativity determination of individual surface atoms by atomic force microscopy. *Nat. Commun.* **8**, 15155 (2017).
18. Hunter, E. P. L. & Lias, S. G. Evaluated gas phase basicities and proton affinities of molecules: an update. *J. Phys. Chem. Ref. Data* **27**, 413–656 (1998).
19. Gorte, R. J. & White, D. Interactions of chemical species with acid sites in zeolites. *Top. Catal.* **4**, 57–69 (1997).
20. Larrazábal, G. O., Shinagawa, T., Martín, A. J. & Pérez-Ramírez, J. Microfabricated electrodes unravel the role of interfaces in multicomponent copper-based CO_2 reduction catalysts. *Nat. Commun* **9**, 1477 (2018).
21. Martin, O. et al. Indium oxide as a superior catalyst for methanol synthesis by CO_2 hydrogenation. *Angew. Chem. Int. Ed.* **128**, 6369–6373 (2016).
22. Hagleitner, D. R. et al. Bulk and surface characterization of In_2O_3(001) single crystals. *Phys. Rev. B* **85**, 115441 (2012).
23. Wagner, M. et al. Reducing the In_2O_3(111) surface results in ordered indium adatoms. *Adv. Mater. Interfaces* **1**, 1400289 (2014).
24. Capdevila-Cortada, M., Vilé, G., Teschner, D., Pérez-Ramírez, J. & López, N. Reactivity descriptors for ceria in catalysis. *Appl. Catal. B* **197**, 299–312 (2016).
25. Wagner, M. et al. Resolving the structure of a well-ordered hydroxyl overlayer on In_2O_3(111): nanomanipulation and theory. *ACS Nano* **11**, 11531–11541 (2017).
26. Yurtsever, A. et al. Understanding image contrast formation in TiO_2 with force spectroscopy. *Phys. Rev. B* **85**, 125416 (2012).
27. Stetsovych, O. et al. Atomic species identification at the (101) anatase surface by simultaneous scanning tunnelling and atomic force microscopy. *Nat. Commun.* **6**, 7265 (2015).
28. Sugimoto, Y. et al. Quantum degeneracy in atomic point contacts revealed by chemical force and conductance. *Phys. Rev. Lett.* **111**, 106803–106805 (2013).
29. Kowalski, P. M., Meyer, B. & Marx, D. Composition, structure, and stability of the rutile TiO_2(110) surface: oxygen depletion, hydroxylation, hydrogen migration, and water adsorption. *Phys. Rev. B* **79**, 115410 (2009).
30. Lackner, P. et al. Water adsorption at zirconia: from the ZrO_2(111)/Pt_3Zr(0001) model system to powder samples. *J. Mater. Chem. A* **6**, 17587–17601 (2018).

Methods

Experiments

The experiments were carried out in two different ultrahigh vacuum chambers of a similar design, each one based on a two-vessel system with base pressures of $<2\times10^{-10}$ mbar and $<2\times10^{-11}$ mbar in the preparation and analysis chambers, respectively. The preparation chambers contain standard surface cleaning and heating facilities. The analysis chambers are equipped with a low-temperature STM/AFM (Omicron) head and a Tribus (ScientaOmicron) head, respectively, using qPlus sensors[10] and low-noise amplifiers[31,32]. Tips were electrochemically etched from a 25-µm-thick tungsten wire. The measurements were performed at a sample temperature of around 5 K. The images and $F(z)$ curves were recorded with different sensors, defined by their resonance frequency f_R, spring constant k and quality factor Q: (1) $f_R = 31$ kHz, $k = 2{,}000$ N m^{-1}, $Q \approx 36{,}000$; (2) $f_R = 47.5$ kHz, $k = 3{,}750$ N m^{-1}, $Q \approx 15{,}000$; (3) $f_R = 77.7$ kHz, $k = 5{,}400$ N m^{-1}, $Q \approx 71{,}000$. In constant-height nc-AFM, typical oscillation amplitudes of 50–100 pm were used and a scanning speed corresponding to about 10 min per image. The tip was frequently refreshed on a Cu(100) single crystal and on the In_2O_3 sample using gentle voltage pulses until a frequency shift between 0 and −5 Hz in constant-current STM was obtained on In_2O_3 (setpoint +1 V, 20 pA). The local contact potential difference between the tip and the In_2O_3 surface was close to zero due to the used treatment; the OH-terminated tips typically showed a small local contact potential difference shift of −0.2 V to −0.3 V.

$In_2O_3(111)$ single crystals[22] were prepared by cycles of sputtering (1 keV Ar^+) and annealing at 450–500 °C in 6×10^{-7} mbar oxygen as described in ref. [23]. The clean surface was characterized with STM and AFM before the water adsorption experiments. Rutile $TiO_2(110)$ single crystals were prepared by the same procedure; here an annealing temperature of 720 °C was applied. Zirconium oxide thin films were prepared by oxidation of a $Pt_3Zr(0001)$ alloy, as described in ref. [30].

Adsorption of low water doses results in hydroxyls as previously described in refs. [25,26,30] for In_2O_3, TiO_2 and zirconium oxide/Pt_3Zr, respectively. Water was dosed via a high-precision leak valve from a glass tube containing a few millilitres of distilled water (Milli-Q). Before the experiments, the water was degassed by several freeze–pump–thaw cycles and the purity was checked with a quadrupole mass spectrometer.

The $O_SH(\beta)$ that form when water dissociates on $In_2O_3(111)$ were manipulated with the STM/AFM tip. This causes the H atom to desorb from the surface as described in ref. [25], or, though much less probable, to re-adsorb on a nearby surface O(3c), thereby forming a new O_SH group. The most successful way was voltage pulses during conventional STM imaging. The window for re-adsorption is approximately 0.1 V below the parameters for complete desorption (which are +2.8 V at an STM setpoint of 30 pA and +1.0 V) and slightly tip dependent; examples are provided in the Extended Data Fig. 5.

The force–distance curves were acquired by imaging in constant-height AFM mode and pausing the tip at a z position close to the force minimum of the O_WH. The tip was then retracted by about 1.2 nm to cover a sufficiently wide range of the long-range interaction. Conversion of the frequency-shift signal to forces was performed using ref. [33]. The long-range forces[14] were treated by subtracting averaged background $F(z)$ curves measured in the same experiment on the $In_2O_3(111)$ surface in-between the OH groups, that is, mostly in regions A and C of the unit cell (Fig. 1a). Extended Data Fig. 6 describes how the long-range interaction forces are subtracted from the curves. All displayed curves are averaged spectra of multiple repetitions on the same OH group or, for O_WH and O_SH, also on different ones.

Theory

DFT calculations were carried out with the plane-wave code PWscf of the Quantum ESPRESSO software package[34] using the Perdew–Burke–Ernzerhof (PBE) exchange-correlation functional[35], Vanderbilt ultrasoft pseudopotentials[36] and a plane-wave kinetic energy cut-off of 30 Rydberg. The In 4d and the Ti 3s,3p electrons were treated as valence states. The same setup was used as in our previous work, see refs. [23,25,29,37]. The van der Waals forces between the AFM tip and the substrate were included by using the Grimme D3 dispersion correction with Becke–Johnson damping[38].

The $In_2O_3(111)$ surface structures were represented by a symmetric slab with a thickness of four O_{12}–In_{16}–O_{12} trilayers. The calculated theoretical bulk lattice constant of 10.276 Å was used for the in-plane dimensions of the periodically repeated slabs, which were separated by an 18-Å vacuum region. In the AFM calculations, the thickness of the vacuum region was increased to 36 Å to accommodate the tip.

The adsorption of water and the displacement of protons were studied first with a primitive (1 × 1) surface unit cell (160 atoms without adsorbates, lateral dimension 14.532 Å). In this cell, a displaced proton always stays next to the water triangle/propeller where it originates from. To study also the situation where a proton is displaced to a neighbouring, intact water triangle/propeller, calculations were repeated for a three-times-larger (√3 × √3) unit cell (480 atoms, lateral dimension 25.171 Å). For the smaller cell, a (2,2,1) Monkhorst–Pack k-point mesh was used, whereas the Γ point was sufficient for the larger cell. An initial set of AFM calculations was done with the (1 × 1) unit cell. All final results, however, were obtained for the larger (√3 × √3) cell. In the geometry optimizations, the bottom two trilayers of the slab were kept fixed. Only the atoms in the upper two trilayers together with the adsorbed water molecules were relaxed, using a force convergence threshold of 5 meV Å^{-1}.

Calculations for the rutile $TiO_2(110)$ surface were done with a slab of five O–Ti_2O_2–O trilayers and a (4 × 2) surface unit cell (240 atoms, lateral dimensions 11.864 Å × 13.141 Å), using a (2,2,1) Monkhorst–Pack k-point mesh. The in-plane dimensions of the slab are based on the calculated rutile TiO_2 bulk lattice constants of a = 4.646 Å and c = 2.966 Å. The vacuum region had a similar thickness to that in the In_2O_3 calculations. The atoms at the bottom of the slab were saturated by pseudo-hydrogen atoms[29]. The pseudo-hydrogen atoms together with the bottom two trilayers of the slab were kept fixed in the geometry optimizations and only the upper three trilayers were allowed to relaxed.

The adsorption energy of H atoms, E^H_{ads}, was calculated with respect to the H_2 molecule, that is, $E^H_{ads} = E^H_{slab} - E^{ref}_{slab} - \frac{1}{2}E^{H_2}_{mol}$.

The PA of a surface site O is defined as the enthalpy change of the deprotonation reaction in the gas phase

$$X\text{–}OH_{(g)} \rightarrow X\text{–}O^-_{(g)} + H^+_{(g)}$$

The closely related gas-phase basicity ΔG_{GPB} is the Gibbs free energy change for the same gas-phase reaction. PA and ΔG_{GPB} are thus measures for the gas-phase acidity of X–OH. In contrast, pK_a is derived from the Gibbs free energy change of deprotonation ΔG_{acid} in a liquid environment. ΔG_{acid} differs from the gas-phase basicity by including the solvation free energies ΔG_{sol} of all participating species and can be derived by a thermodynamic cycle:

$$\begin{array}{ccc} X\text{–}OH_{(g)} & \xrightarrow{\Delta G_{GPB}} & X\text{–}O^-_{(g)} + H^+_{(g)} \\ \Delta G_{sol}(X\text{–}OH)\downarrow & & \Delta G_{sol}(X\text{–}O^-)\downarrow \quad \downarrow \Delta G_{sol}(H^+) \\ X\text{–}OH_{(aq)} & \xrightarrow{\Delta G_{acid}} & X\text{–}O^-_{(aq)} + H^+_{(aq)} \end{array}$$

The acid dissociation constant pK_a is the negative logarithm of the corresponding equilibrium constant K

$$K = e^{-\Delta G_{acid}/k_BT} \text{ and } pK_a = -\log K,$$

where k_B is the Boltzmann constant and T is temperature. Note the small energy scale: at room temperature, a change of only 6 kJ mol^{-1} in the Gibbs free energy ΔG_{acid} leads to a shift of the pK_a value by one unit.

An extensive search was performed to find a realistic atomistic model for the AFM tip. Several tip models with different structure and composition were considered. Many tip models were unstable in initial test calculations of the $F(z)$ curves: some of them lost their terminal OH group, or protons were transferred from the surface to the tip (converting the terminal OH group into a water molecule). For a stable tip, which is able to describe the experimentally measured $F(z)$ curves, it is mandatory to find a structure that is not too reactive. Good criteria for a chemically inert tip are high coordination numbers of the atoms and a large gap between the highest occupied molecular orbital (HOMO) and the lowest unoccupied molecular orbital (LUMO). The final AFM tip used in all calculations is based on a water-saturated In_2O_3 cluster. Its structure is described in Extended Data Fig. 9.

In the calculations of the force–distance curves $F(z)$, we followed closely the procedures of the AFM experiments. The tip was initially placed at a vertical position z close to the force minimum, with its centre above the O atom of a particular OH group (see choice of $z = 0$ in the AFM experiments). Then, a geometry optimization was performed in which the top atoms of the tip were kept fixed and only the In atom at the tip apex together with its four OH groups were allowed to relax (Extended Data Fig. 9c). Within the slabs, the same atoms were fixed/relaxed as in the initial geometry optimization without tip.

Starting from the initial height, the z coordinate of the AFM tip was increased and decreased in steps of 0.1 Å. The atomic positions of the previous step were used as initial configuration in the geometry optimization of the subsequent step. At larger z distances, the step size was increased to 0.24 Å. This procedure was typically repeated for 50 z values. The result of the whole sequence is shown for two examples (the O_WH and $O_SH(\beta)$ groups on $In_2O_3(111)$ and one tip orientation) in the Supplementary Information. At each tip height z, the energy $E(z)$ of the optimized geometry was recorded. The energy minimum in the $E(z)$ curve was determined by a polynomial fit to a few neighbouring data points. For the tip height at the energy minimum, the structure was re-optimized and the bond lengths reported in Fig. 3 were calculated. The $F(z)$ curves were obtained by fitting a spline to $E(z)$ and taking the derivative. Jumps in the $F(z)$ curves were frequently observed, which were caused by the re-orientation of the tip OH group or an OH at the surface. The new local energy minimum structure was then used as starting point for the calculation of a new $E(z)$ curve following the iterative procedure described above.

As only weak interactions are analysed, and the van der Waals background represents a substantial contribution, the calculated $F(z)$ curves were background corrected in the same way as in the experiment: additional $F(z)$ curves were calculated above the high-symmetry sites A and C at the hydroxylated and the water-free $In_2O_3(111)$ surface using two different azimuthal orientations of the tip (Extended Data Fig. 10). On the hydroxylated surface, the A and C sites are as far away as possible from the adsorbed water molecules. The curves were averaged and subtracted from all $F(z)$ curves calculated above surface OH groups (Fig. 2b).

For the calculation of force–distance curves for the $O_SH(\alpha)$, $O_SH(\gamma)$ and $O_SH(\delta)$ groups, a proton was displaced on the hydroxylated $In_2O_3(111)$ surface from $O_SH(\beta)$ to the respective surface site. A (1×1) surface unit cell contains three O atoms of each type α, γ and δ. Thus, nine different O_SH groups can be formed, which are all symmetry inequivalent as the displacement of the proton breaks the three-fold symmetry of the initial triangle/propeller-like water structure. Calculations were performed for all nine O_SH groups. In addition, for each surface OH (including $O_SH(\beta)$ and O_WH), six different orientations of the AFM tip were considered, with the terminating OH group of the tip pointing in different azimuthal directions rotated by 60°. Some of the calculated $F(z)$ curves turned out to be identical as the OH group of the tip rotated into the same direction in the geometry optimizations. A selected set of the final distinctly different 25 $F(z)$ curves is shown in Fig. 2b. The scatter in the curves demonstrates the uncertainty due to specific surface site and tip orientation. Each of the $F(z)$ curves can be assigned unambiguously to one of three classes corresponding to the three types of surface OH group, $O_SH(\alpha)$, $O_SH(\gamma)$ and $O_SH(\delta)$. Curves within each class were averaged and are discussed in the main text. The three-times-larger $(\sqrt{3} \times \sqrt{3})$ surface unit cell offers 27 different sites for a displaced proton from an $O_SH(\beta)$ group, 9 of each type α, γ and δ. Here force–distance curves were calculated for only a selected set of possible O_SH groups. The selection was based on the results from the (1×1) unit cell and on the observed manipulations in the STM/AFM experiments.

In the case of the rutile $TiO_2(110)$ surface, OH groups were introduced by adding one or two H atoms on top of a bridging surface O atom to the supercell. This represents the structure that is formed in experiment by the dissociative adsorption of water molecules at the O vacancies of the rutile $TiO_2(110)$ surface[26]. Force–distance curves were calculated with the same AFM tip model as for In_2O_3, also considering different tip orientations. However, only two stable orientations of the OH group at the tip apex were found, both are equivalent due to the mirror symmetry of the surface. Therefore, only two $F(z)$ curves are shown in Extended Data Fig. 7b, stemming from the supercell calculations with one and with two H atoms.

Finally, $F(z)$ curves were calculated for each of the probe molecules, again using the same AFM tip as in the surface calculations while keeping the geometries, the overall procedure and all calculation parameters as similar as possible. The same supercell was used, and the probe molecules were oriented such that their OH group pointed towards the AFM tip. As in the surface calculations, different orientations of the AFM tip with respect to the OH axis of the molecule were probed.

Data availability

The datasets generated and analysed during the current study are available from the corresponding author on reasonable request.

31. Huber, F. & Giessibl, F. J. Low noise current preamplifier for qPlus sensor deflection signal detection in atomic force microscopy at room and low temperatures. *Rev. Sci. Instrum.* **88**, 073702 (2017).
32. Štubian, M., Bobek, J., Setvín, M., Diebold, U. & Schmid, M. Fast low-noise transimpedance amplifier for scanning tunneling microscopy and beyond. *Rev. Sci. Instrum.* **91**, 074701 (2020).
33. Sader, J. E. & Jarvis, S. P. Accurate formulas for interaction force and energy in frequency modulation force spectroscopy. *Appl. Phys. Lett.* **84**, 1801–1803 (2004).
34. Giannozzi, P. et al. Quantum ESPRESSO: a modular and open-source software project for quantum simulations of materials. *J. Phys. Condens. Matter* **21**, 395502 (2009).
35. Perdew, J., Burke, K. & Ernzerhof, M. Generalized gradient approximation made simple. *Phys. Rev. Lett.* **77**, 3865–3868 (1996).
36. Vanderbilt, D. Soft self-consistent pseudopotentials in a generalized eigenvalue formalism. *Phys. Rev. B* **41**, 7892–7895 (1990).
37. Wagner, M. et al. Well-ordered In adatoms at the $In_2O_3(111)$ surface created by Fe deposition. *Phys. Rev. Lett.* **117**, 206101 (2016).
38. Grimme, S., Antony, J., Ehrlich, S. & Krieg, H. A consistent and accurate ab initio parametrization of density functional dispersion correction (DFT-D) for the 94 elements H–Pu. *J. Chem. Phys.* **132**, 154104 (2010).
39. Sokolović, I. et al. Resolving the adsorption of molecular O_2 on the rutile $TiO_2(110)$ surface by noncontact atomic force microscopy. *Proc. Natl Acad. Sci. USA* **117**, 14827–14837 (2020).
40. Hapala, P. et al. Mechanism of high-resolution STM/AFM imaging with functionalized tips. *Phys. Rev. B* **90**, 085421 (2014).
41. Linstrom, P. J. & Mallard, W. G. (eds) *NIST Chemistry WebBook: NIST Standard Reference Database Number 69* (National Institute of Standards and Technology, 2018); https://webbook.nist.gov/chemistry.

Acknowledgements This work was supported by the Austrian Science Fund (FWF), project V 773-N (Elise-Richter-Stelle, M.W.) and Z 250-N27 (Wittgenstein Prize, U.D.), as well as the German Research Foundation (DFG), Research Unit FOR 1878 (funCOS, B.M.). M.W. and U.D. also acknowledge funding under the Horizon 2020 Research and Innovation Programme under the grant agreement number 810626. M. Setvin acknowledges the support of GAUK Primus/20/SCI/009. Computational resources were provided by LRZ Garching (project pn98fa)and RRZ Erlangen.

Author contributions M.W. and M. Setvin conducted the experiments. M.W., M. Setvin and M. Schmid analysed the AFM data. B.M. performed the calculations and derived the scaling relationships. M.W., B.M. and U.D. wrote the manuscript, which was reviewed and edited by all authors. U.D. oversaw the project.

Competing interests The authors declare no competing interests.

Additional information

Supplementary information The online version contains supplementary material available at https://doi.org/10.1038/s41586-021-03432-3.

Correspondence and requests for materials should be addressed to U.D.

Peer review information *Nature* thanks Leo Gross and the other, anonymous, reviewer(s) for their contribution to the peer review of this work.

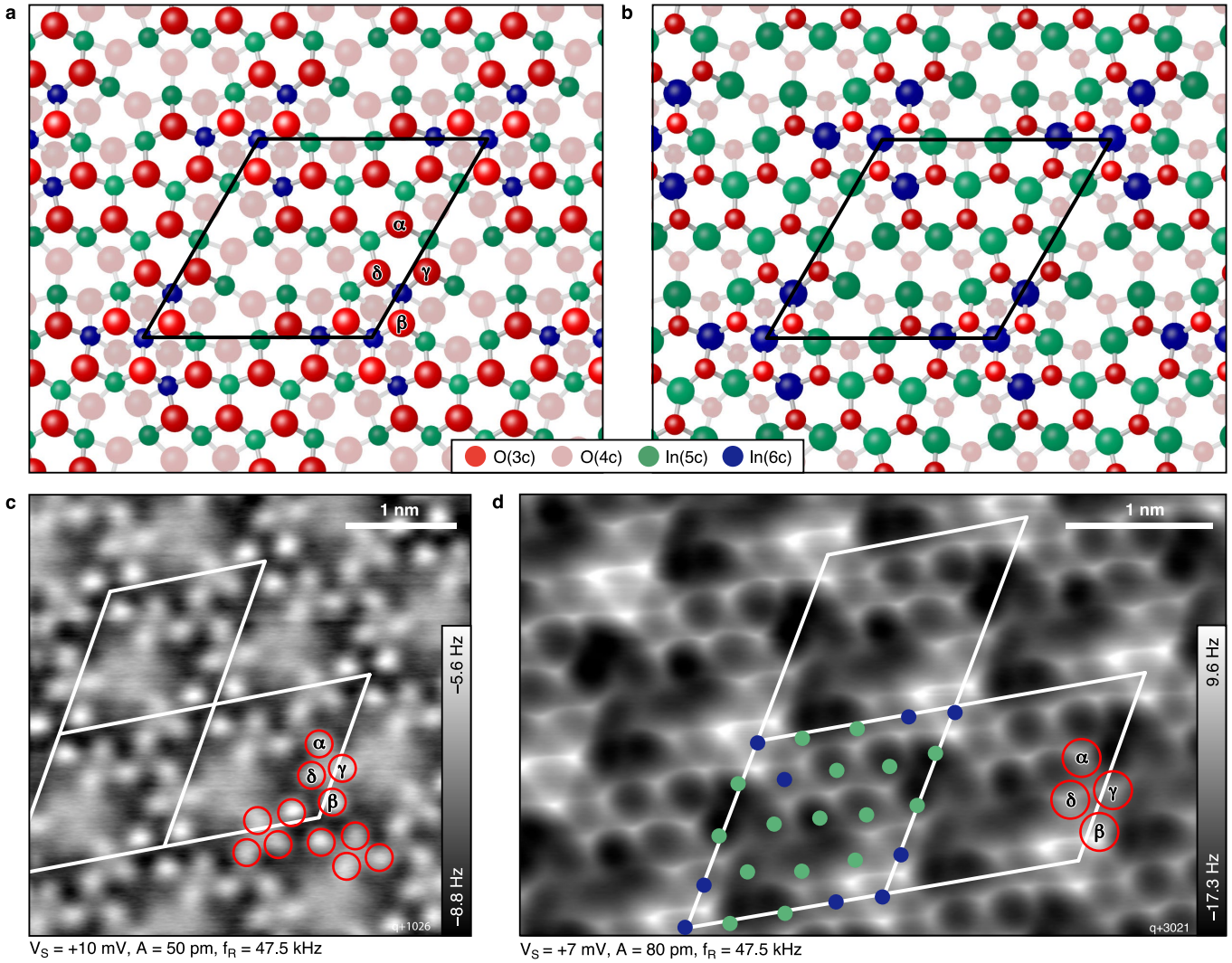

V_S = +10 mV, A = 50 pm, f_R = 47.5 kHz

V_S = +7 mV, A = 80 pm, f_R = 47.5 kHz

Extended Data Fig. 1 | The clean In_2O_3(111) surface imaged with various AFM tip terminations. a, **b**, Structural models of the In_2O_3(111) surface, with emphasis on the surface O (red) atoms (**a**) and In (blue, green) atoms (**b**). Also indicated is the unit cell. **c**, AFM image with an O-terminated tip. The intentional functionalization was performed on a reduced rutile TiO_2(110) surface with adsorbed O_2 molecules by applying voltage pulses (approximately +3 V) above the molecular oxygen species. Previous experience has shown that such a tip functionalization provides excellent resolution of the oxygen sublattice in the repulsive regime[39]. Such tips provide negligible attractive interaction with the anion lattice and they are rigid; the resulting images are therefore not distorted by bending the tip apex[40] and clearly show the O sublattice, O(α) to O(δ). **d**, AFM image taken after the tip was gently pushed into the hydroxylated In_2O_3(111) surface to induce an OH termination. The more flexible tip termination leads to crests in the images. The dark, round features correspond to In, which are indicated by the green and blue dots (attractive interaction between negatively charged (tip) OH and In anions). The bright maxima correspond to O(3c).

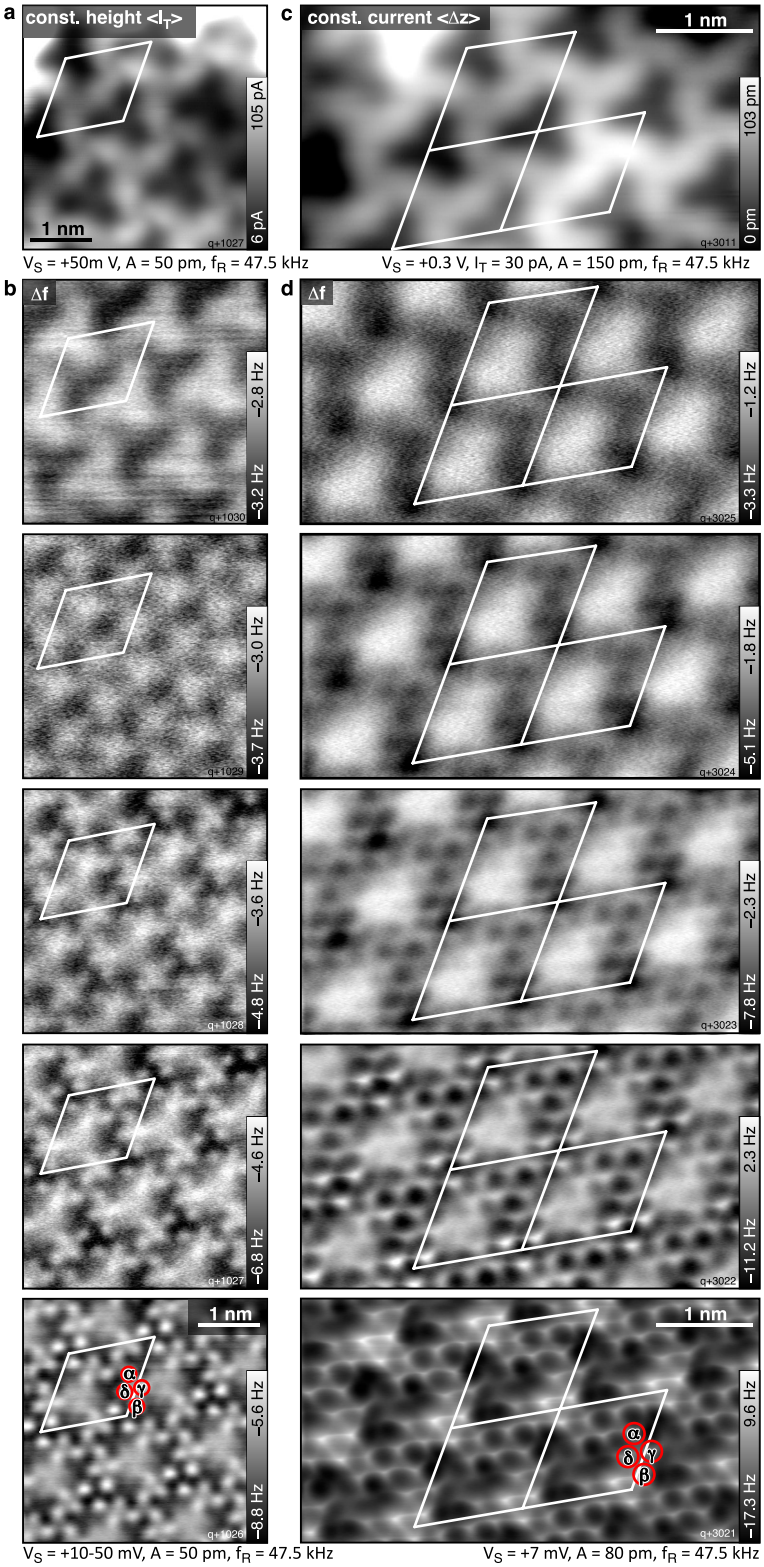

Extended Data Fig. 2 | Distance-dependent STM/AFM images of the clean In_2O_3(111) surface. a, **b**, O-terminated tip. **a**, Constant-height STM image (tunnelling current, I_T). **b**, Constant-height AFM images (frequency shift, Δf). From top to bottom, the tip–sample distance was progressively reduced in steps of about 50 pm. **c**, **d**, OH-terminated tip. **c**, Constant-current STM image. **d**, Same as **c** but the distance was reduced in steps of about 40 pm.

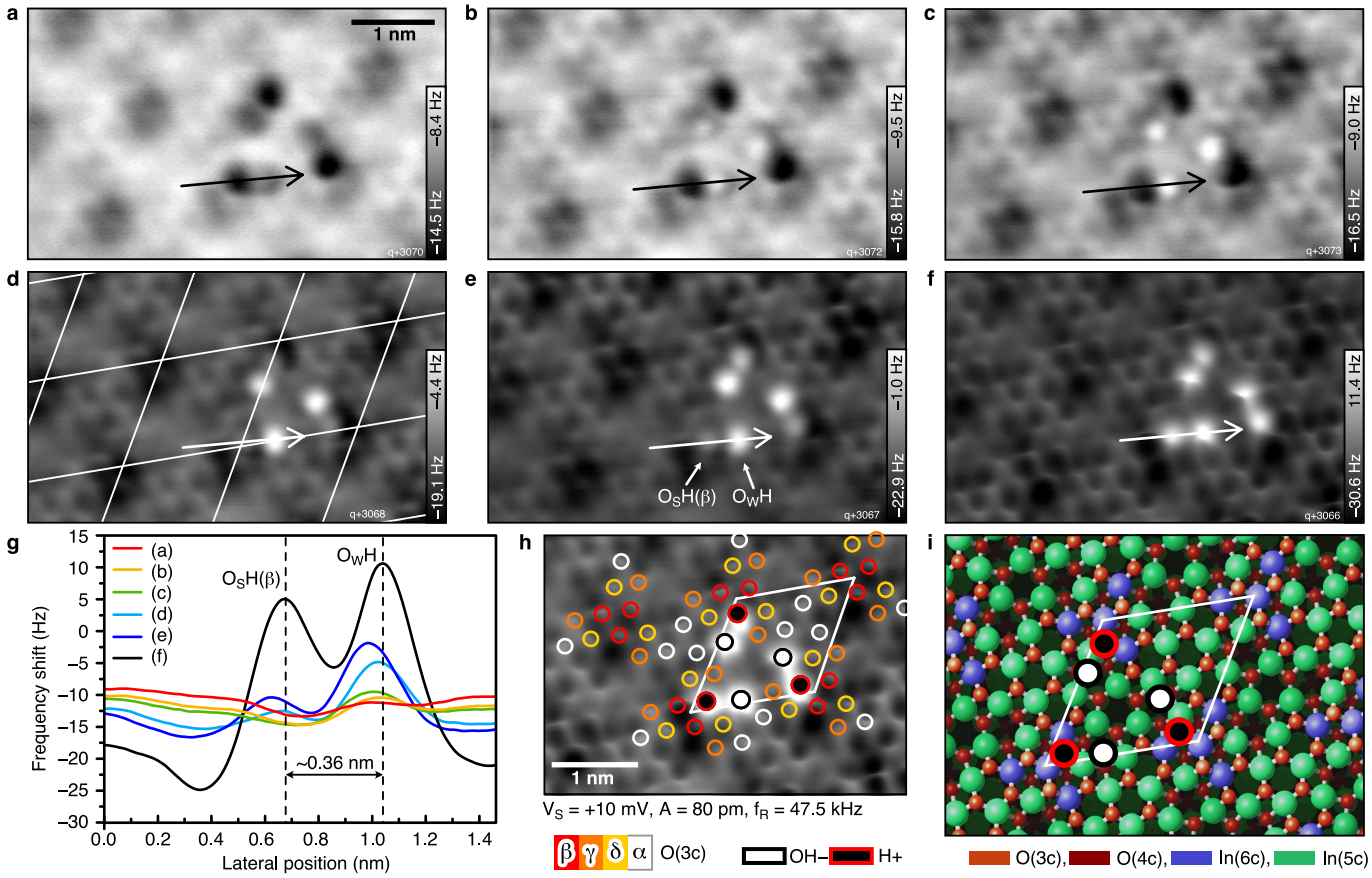

Extended Data Fig. 3 | Adsorption sites of OH groups on In_2O_3(111). **a**–**f**, Constant-height nc-AFM images of three dissociated water molecules in adjoining unit cells, taken with decreasing tip height. The height difference Δz between the subsequent images is 10 to 15 pm. Each dissociated water molecule gives rise to two OH groups adsorbed next to each other, O_WH and O_SH (where the 'W' and 'S' indicate the origin of the oxygen atom, that is, the water molecule or the surface, respectively)[25]. In **a**, with the tip farthest away, both OH groups are imaged as dark features. As the tip comes closer to the OH groups (**b**, **c**), the O_WH (sticking farther away from the surface than the O_SH) turn bright (onset of repulsive interaction, but overall attractive forces). In **d**, the O_SH also start to be imaged as bright features. Approaching the surface even more, **e**, **f** reveal the O(3c) lattice atoms of the surface; this information was used to determine the adsorption sites of the OH groups experimentally. **g**, Profiles of the frequency shift across the O_SH and O_WH pair as indicated by the arrows in **a**–**f**. **h**, Same image as **f** with the O(3c) lattice superimposed (O(α), white; O(β), red; O(γ), orange; O(δ), yellow). The site of the O_SH is identified as an O(β) (circle filled black). **i**, Atomic model of the surface including the adsorption sites of the O_SH and O_WH (black circle, filled white), which bridges two In(5c) atoms nearby. The adsorption sites agree with previous STM and DFT results in ref. [25].

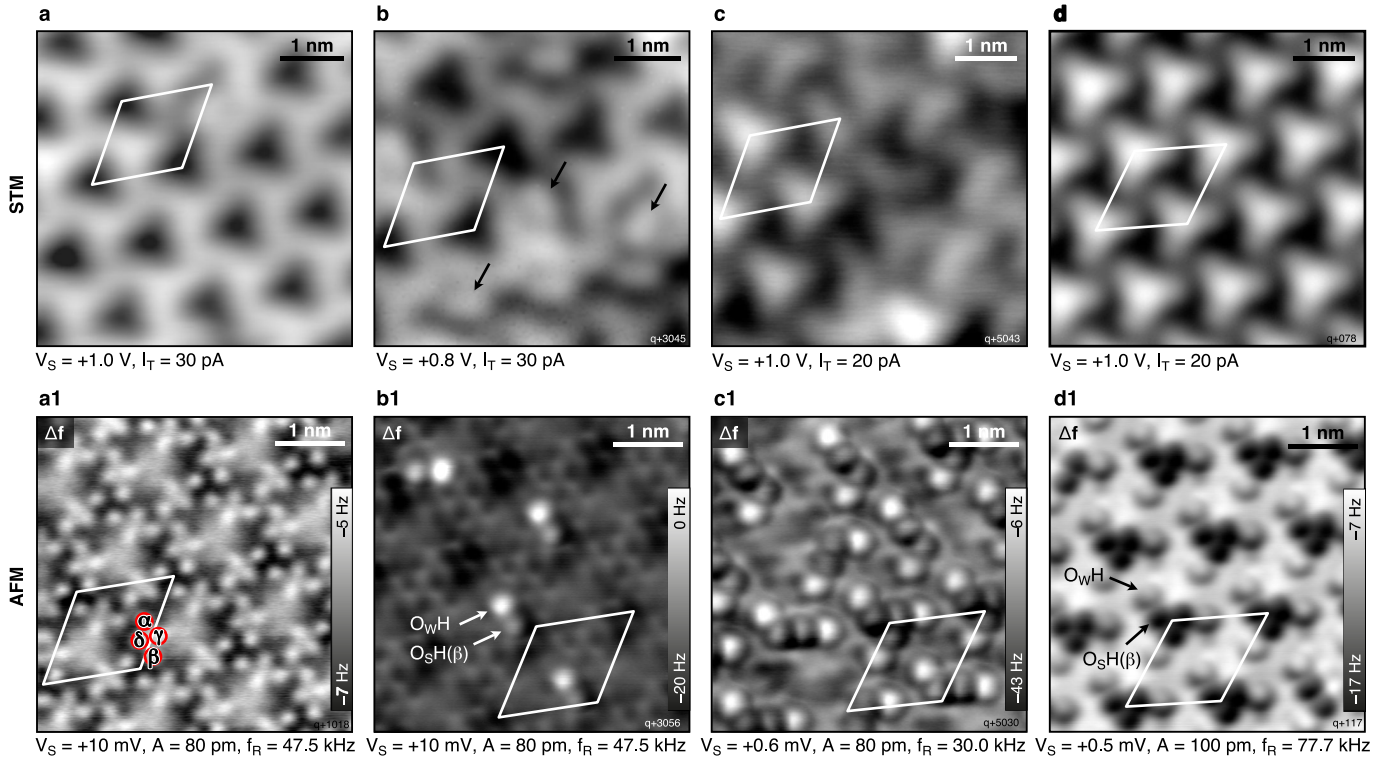

Extended Data Fig. 4 | The hydroxylated In_2O_3(111) surface with increasing water coverages in STM and AFM. The STM (top) and AFM images (bottom) were acquired at different regions of the surface. **a1**, Oxygen-terminated tip. **b1**–**d1**, OH-terminated tips. **a**, **a1**, Clean In_2O_3(111) surface. The contrast in STM (empty states) is dominated by the high density of states of the In(5c) and the lower density of states at the In(6c), which gives dark triangles. In AFM, the contrast is dominated by the topmost atoms of the surface, that is, the 12 O(3c) per unit cell. **b**, **b1**, Single dissociated water molecules, O_WH and O_SH. **c**, **c1**, Two and three dissociated water molecules per unit cell. **d**, **d1**, Saturation with three dissociated water molecules per unit cell in symmetry-equivalent sites, giving rise to a 'propeller-like feature' consisting of three brighter (O_WH) and darker (O_SH at O(β) site) at equivalent positions. For DFT calculations and structural relaxations see ref. [25].

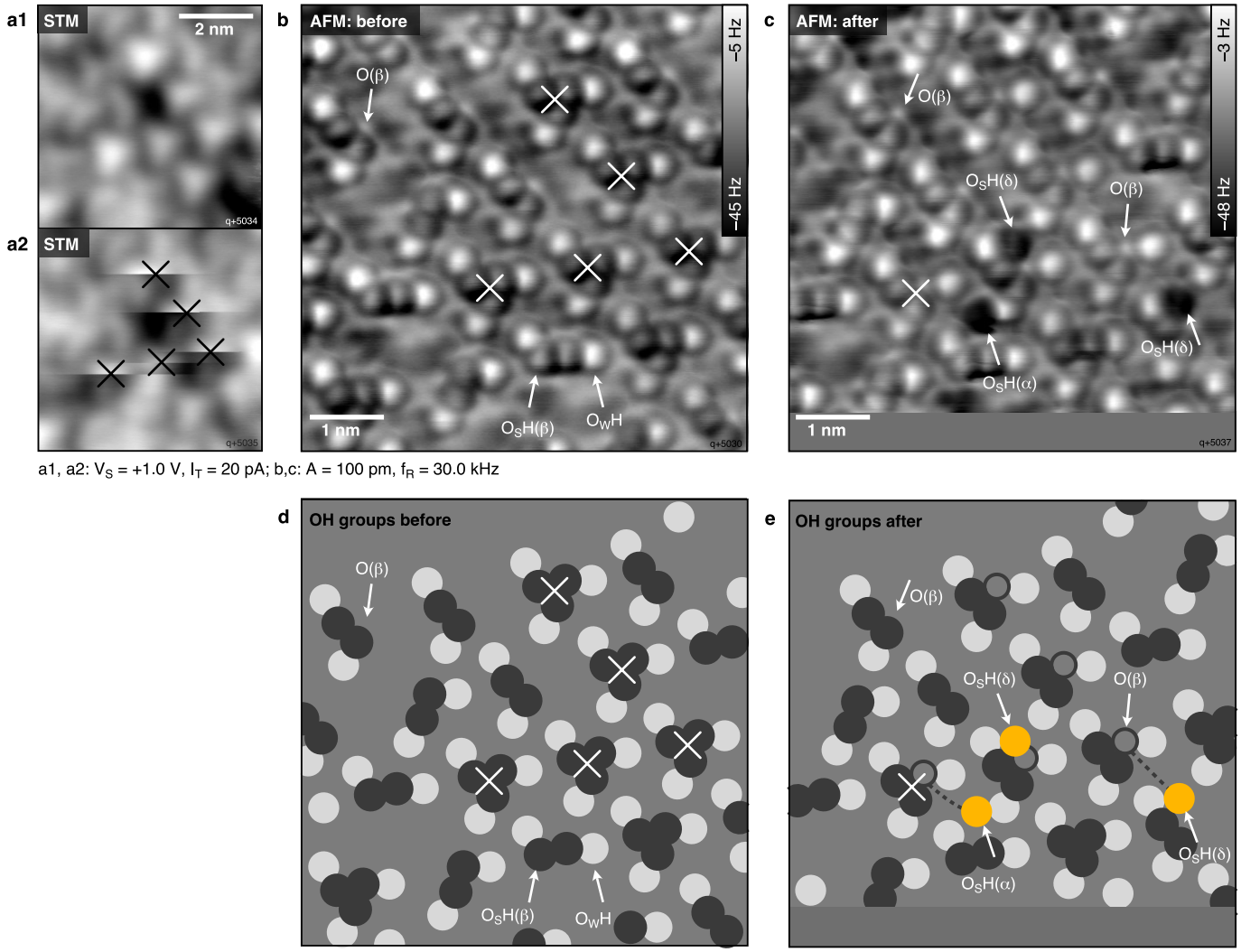

a1, a2: V_S = +1.0 V, I_T = 20 pA; b,c: A = 100 pm, f_R = 30.0 kHz

Extended Data Fig. 5 | Manipulation of O_SH groups by voltage pulses. a, STM image before (**a1**) and during (**a2**) the manipulation. Five pulses (two times +2.8 V and three times +2.7 V, 20 pA, marked with crosses) were applied during STM imaging in the centre of individual propeller-like structures. **b**, **c**, AFM image of the same surface area before the manipulation (**b**; with crosses marking the position of the pulses) and after the manipulation (**c**). **d**, **e**, Cartoons identifying the various species before (**d**) and after (**e**) the manipulation. In each manipulation, one H per propeller was removed, leaving behind a denuded O(β), indicated in **e** and visible as a smaller, bright dot in the AFM image in **c**. Two H have desorbed and three H have re-adsorbed, visible as very dark features in AFM in **c** and indicated in yellow in **e**.

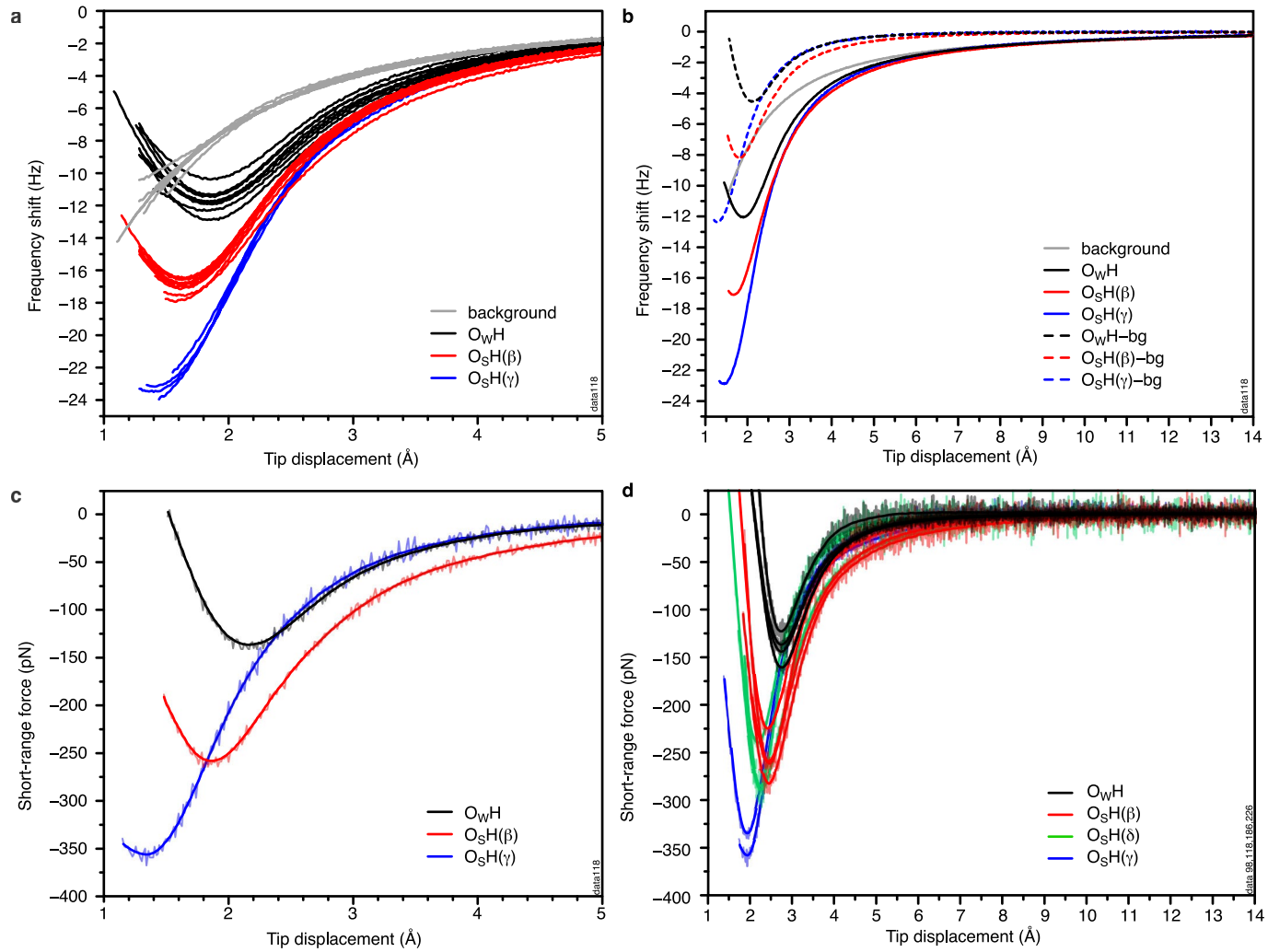

Extended Data Fig. 6 | Data evaluation of *F*(*z*) curves. a, Frequency-shift curves acquired on different OH groups and the In_2O_3(111) background measured in-between the OH groups (mostly in regions A and C, see Fig. 1). **b**, The averaged curves from **a** (solid lines) and after background subtraction (dashed lines). **c**, Background-corrected *F*(*z*) curves obtained from **b** using Sader's formula[33] (f_R = 77.7 kHz, k = 5,400 N m^{-1}, A = 100 pm). **d**, The *F*(*z*) curves of Fig. 2a showing the whole *z* range.

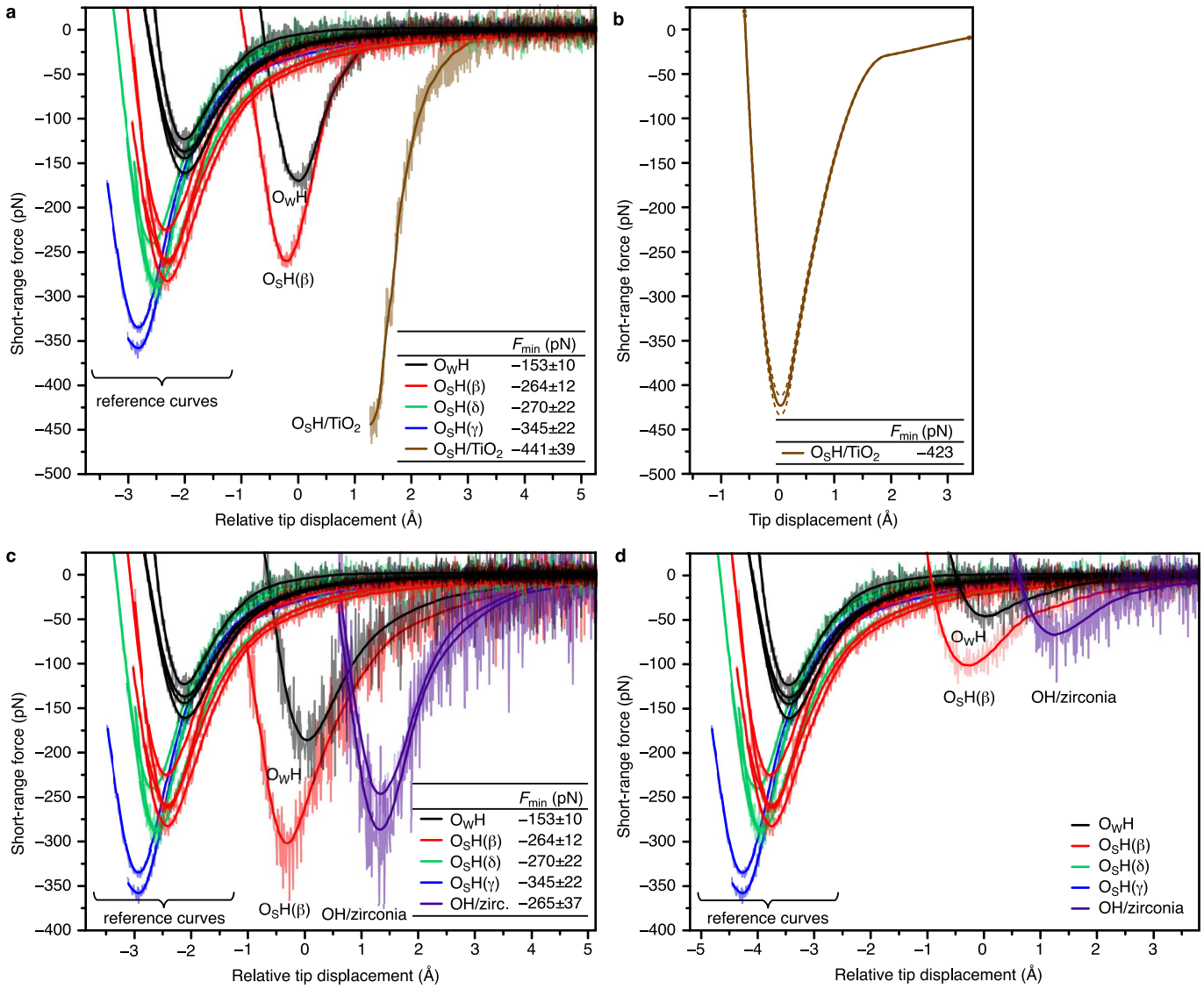

Extended Data Fig. 7 | Transferability and reproducibility of the method. $F(z)$ curves on $O_SH/TiO_2(110)$ and OH/zirconium oxide/$Pt_3Zr(0001)$ obtained with the OH-terminated indium oxide tip. **a**, $TiO_2(110)$: experimental data. The tip was prepared on hydroxylated $In_2O_3(111)$, and $F(z)$ curves were taken on the O_WH and $O_SH(\beta)$ (labelled as such) to ascertain the tip termination ($f_R = 69.6$ kHz, $k = 5{,}400$ N m^{-1}, $A = 60$ pm). For reference, the curves from the main text (Fig. 2) are also plotted on the left; for better visibility they are shifted horizontally by −2 Å. This tip was used to obtain the $F(z)$ curve on $O_SH/TiO_2(110)$ (brown, shifted to the right). Approaching the O_SH on TiO_2 even closer results in picking up the H. The hydroxylated $TiO_2(110)$ surface was prepared following a well established procedure[26], which results in one type of hydroxyl at a bridging O(2c) atom. **b**, Calculated short-range $F(z)$ curves on bridging hydroxyls on $TiO_2(110)$ for two OH coverages (1/4 and 1/8 monolayer) obtained with the OH-terminated InO_x tip. **c**, Zirconium oxide: the standard tip was prepared on hydroxylated $In_2O_3(111)$, and $F(z)$ curves were taken on the O_WH and $O_SH(\beta)$ (labelled as such) to ascertain the tip termination. For reference, the curves from the main text (Fig. 2) are also plotted on the left; for better visibility they are shifted horizontally by −2 Å. This tip was used to take $F(z)$ curves on hydroxylated zirconium oxide (purple, shifted to the right). **d**, Zirconium oxide: the same type of measurement, but with an unknown tip termination that gives more shallow minima for O_WH and O_SH on hydroxylated $In_2O_3(111)$. Note that both tips measure the same relative positions in the force minima of the strongly bound H on $In_2O_3(111)$ and zirconium oxide, that is, the force on OH/zirconium oxide lies between O_WH and $O_SH(\beta)$ ($f_R = 77.2$ kHz, $k = 5{,}400$ N m^{-1}, $A = 240$ pm (In_2O_3), 250 pm (zirconium oxide)). The ultrathin zirconium oxide layer was prepared following the method of ref. [30]. The surface was exposed to 2 langmuir (1 L = 1.33×10^{-6} mbar s) of water at 320 K.

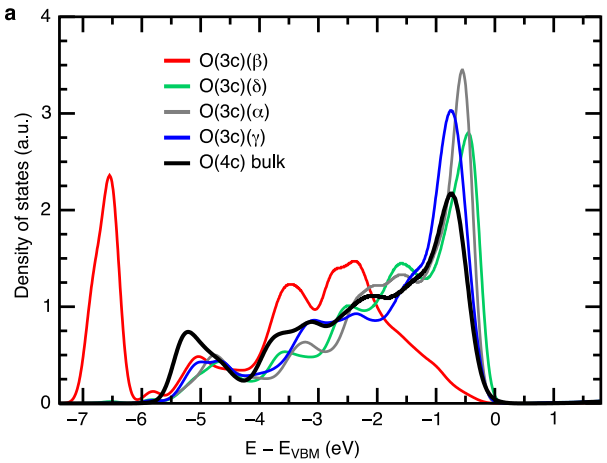

b

Site	E^{H}_{ads} (eV)
O(3c)(δ)	−1.30
O(3c)(α)	−1.24
O(3c)(γ)	−1.05

Extended Data Fig. 8 | Reactivity of the hydroxylated surface. **a**, Atom-resolved PDOS of the four symmetry-inequivalent three-fold coordinated O surface sites on the fully hydroxylated In_2O_3(111) surface with three O_WH and three O_SH(β) per unit cell. The VBM is at 0 eV. **b**, Calculated adsorption energies E^{H}_{ads} for the remaining three unprotonated O(3c) sites (with respect to the H_2 gas phase molecule). The adsorption of water and the formation of the hydroxylated surface structure slightly modifies the reactivity of the unprotonated O(α), O(γ) and O(δ) sites. The saturation of the O(β) sites by protons leads to a strong downward shift of the O(β) 2*p* states. The VBM is now formed by the O(δ) 2*p* states, followed by the O 2*p* states from the O(α) and O(γ) sites. The O(δ), which are the second-most-reactive O species on the uncovered surface, are thus expected to be the most reactive sites on the hydroxylated In_2O_3(111) surface. This is confirmed by the calculated H adsorption energies (**b**). Whereas for O(γ) the H adsorption energies are rather similar on the clean and on the hydroxylated surface, the local relaxations upon water adsorption make the O(α) sites slightly more and the O(δ) slightly less reactive (see **b** and inset in Fig. 1b). As for the clean surface, the pronounced peak in the PDOS of the three-fold coordinated O_S surface atoms at the VBM also leads to an upward shift of their *p*-band centre. The shift of the *p*-band centre has been taken as an indirect measure of surface reactivity[24] and confirms the expected trend in the PA of the different surface sites.

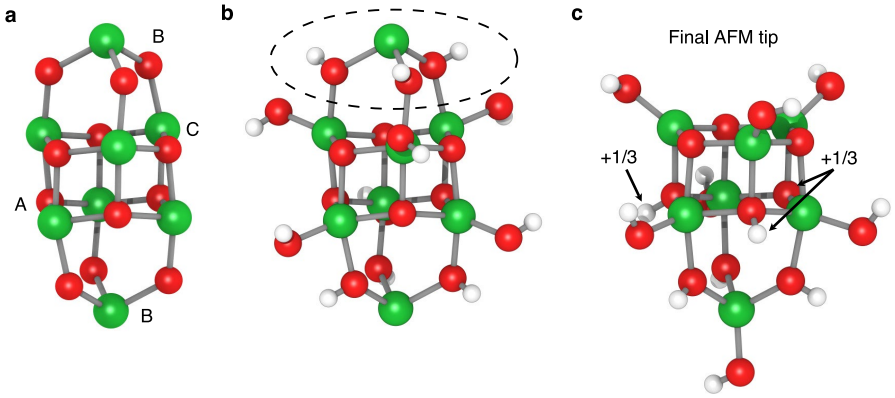

Extended Data Fig. 9 | Tip model for the AFM calculations. a, Relaxed structure of an In_8O_{12} cluster cut out of an $In_2O_3(111)$ slab. The cut is centred around the high-symmetry B site of the surface and its depth is four $In_2O_3(111)$ trilayers. The $In_2O_3(111)$ trilayers are all equivalent but they are shifted such that the high-symmetry sites with a three-fold symmetry axis (see Fig. 1a) form a stacking sequence of BCAB. The cluster consists of an In atom at the B site together with three O atoms, and six-membered In_3O_3 rings around the A and C sites. The cluster is stoichiometric and stable upon geometry optimization, it has a three-fold symmetry axis and its HOMO–LUMO gap is 1.62 eV (PBE). **b**, Cluster after dissociative adsorption of six water molecules to saturate the broken In–O bonds. The OH groups were added to the six In atoms in the two central planes, and the protons were placed on top of the two-fold bridging O atoms. This increased the HOMO–LUMO gap to 2.57 eV. In the next step, the upper $In(OH)_3$ cap was removed (dashed circle). This was done to eliminate the top three-fold coordinated In atom and to reduce the height of the tip model. This saves some computer time in the AFM calculations, as the thickness of the vacuum region can be reduced. Removing the cap increases the HOMO–LUMO gap to 2.68 eV. At this point, the cluster still has a three-fold symmetry axis. **c**, Structure of the final tip. One additional water molecule is added to the cluster (**b**). The OH group is adsorbed at the In apex atom of the tip and the proton is added to one of the remaining O atoms. This breaks the three-fold symmetry of the tip. Careful test calculations showed that the specific choice for the adsorption site of the proton is not important. All tips gave basically the same $F(z)$ curves. In the end, the proton was split into three parts, and three pseudo-hydrogen atoms with nuclear charge of +1/3 were added to the three O atoms closest to the tip apex indicated by arrows. The HOMO–LUMO gap of the final cluster calculated with the PBE functional is 2.64 eV.

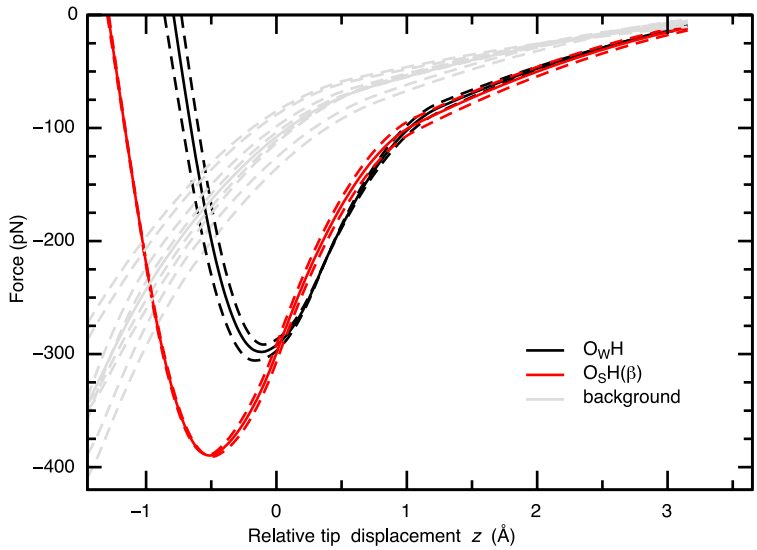

Extended Data Fig. 10 | Illustration of the background subtraction for the calculated *F*(*z*) curves. Grey dashed lines are calculated *F*(*z*) curves at the high-symmetry A and C sites on the hydroxylated and the water-free In_2O_3(111) surface, each for two different azimuthal tip orientations. The average of the eight curves is shown as a grey solid line. In the background-correction procedure, this curve is subtracted from all calculated *F*(*z*) curves above surface OH groups. Black and red graphs show the data for the O_WH and O_SH(β) groups before background subtraction (dashed, calculated curves for two tip orientations; solid, average of the two dashed curves).

a

molecule	PA (kJ/mol)	pK_a
HNO_3 (4)	1368 ± 12	−1.3
H_3PO_4 (1)	1383 ± 21	2.12
HNO_2 (1)	1424 ± 01	3.29
HCOOH (4)	1446 ± 09	3.77
CH_3COOH (4)	1458 ± 08	4.76
C_6H_5COOH (3)	1423 ± 10	4.22
C_6H_5OH (1)	1462 ± 10	9.95
$(CF_3)_3COH$ (1)	1387 ± 09	5.4
$(CF_3)_2CHOH$ (1)	1443 ± 09	9.3
CF_3CH_2OH (1)	1513 ± 10	12.5
HOOH (2)	1574 ± 05	11.6
CH_3CH_2OH (4)	1584 ± 05	15.9
CH_3OH (1)	1597 ± 08	15.5
H_2O (1)	1633 ± 01	15.7

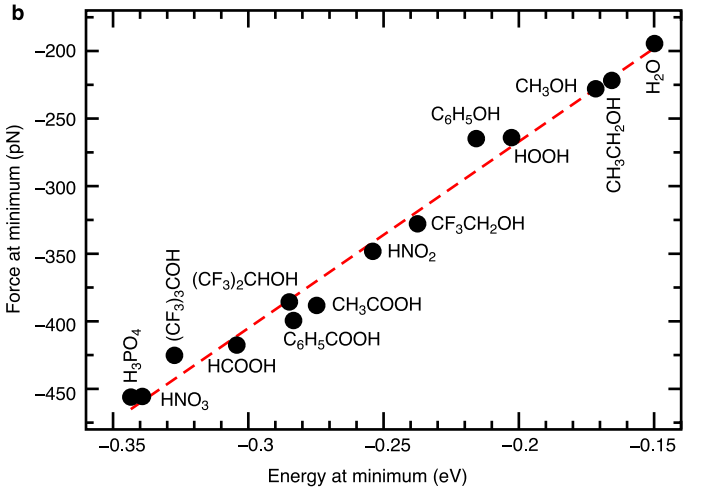

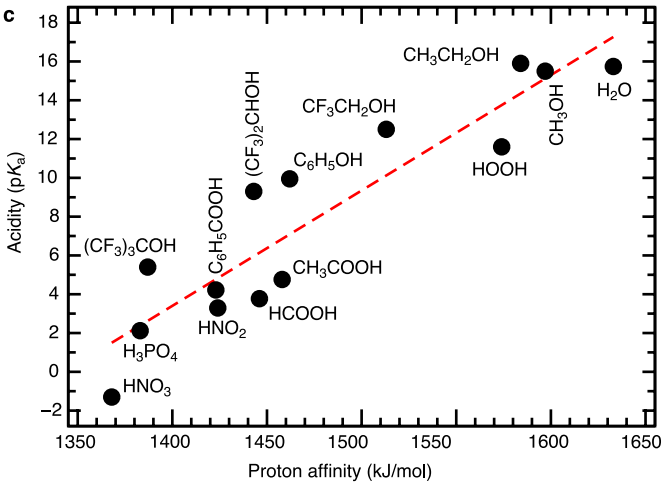

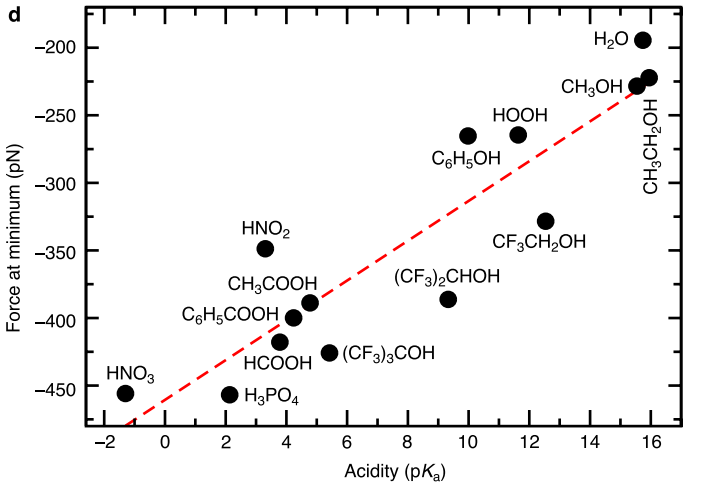

Extended Data Fig. 11 | Correlations between force and energy minima, PA and pK_a, using probe molecules. a, List of probe molecules with their experimental PA and pK_a values. As our aim is to assign PAs to surface O species, only oxygen-based acids and alcohols were selected. The experimental PAs (for the corresponding base, that is, the $X–O^-$ anion) are taken from the National Institute of Standards and Technology (NIST) database[41]. The number of listed NIST entries is given in parenthesis. In case that data from several experiments are available, averaged values and uncertainties are given. **b**, Correlation between force and energy minima. The linear fit to the calculated minima of the $E(z)$ and $F(z)$ curves for our probe molecules (red dashed line) shows an almost perfect linear correlation of the data points. The value of the energy minimum in the $E(z)$ curves (that is, $F(z) = 0$) is the natural measure for the strength of the hydrogen bond that forms between the OH groups of the tip and the molecules. This linear relationship allows us to focus on establishing a correlation between PA or acidity and the force, and not the energy minimum. This is more convenient, because the force minimum is the natural measure from the AFM experiments. Although the energy minimum can be obtained by integrating the $F(z)$ curves, it is not trivial to eliminate ambiguities stemming from a proper choice for the zero point of energy, which determines the integration constant. Furthermore, the force minimum is encountered at a larger OH–tip distance than the energy minimum. The force minimum is therefore less influenced by other interactions between the tip and side groups of the molecule or neighbouring atoms on the surface. **c**, Correlation between the PA and acidity constant pK_a of the selected probe molecules. The PA also governs the pK_a in wet, solution-based chemical processes: an OH group with a strongly bound proton (high PA of the O atom) is a weak acid, and an OH group with a weakly bound proton (low PA of the O atom) is a strong acid. A linear fit (red dashed line) to the experimental data in **a** shows the expected trend, that is, strong acids have a low PA, and weak acids bind their proton more strongly. However, in addition to the PA, the pK_a also includes the Gibbs free energy of solvation of the acid (XOH), the conjugated base (XO^-) and the H^+ (see the thermodynamic cycle in Methods). These species have different solubilities, which leads to a large scatter of the data points. **d**, Correlation between calculated AFM force minima and the experimental acidity constants pK_a of the probe molecules. As expected from the discussion in **c**, the force minima show a larger scatter around the red dashed regression line than when plotted with respect to the PA (see Fig. 4). This is because the AFM measurements are done in vacuum and do not include information about solvation free energies. Thus, the prediction of absolute pK_a values for our OH groups on the $In_2O_3(111)$ surface based on the AFM measurements alone is not possible. Still, there is a clear trend that strong acids form strong H bonds with the AFM tip (deep force minimum, low PA), whereas weak acids form weak H bonds (shallow force minimum, high PA). If we assume that the solvation energies of the structurally rather similar OH groups do not differ too much, then the deviation from the regression line would be similar for all of them, which would allow us to predict at least relative pK_a changes between the OH groups by using the slope of the linear regression. The AFM-measured difference in the force minima of 81 pN for the $O_SH(\beta)$ and $O_SH(\gamma)$ sites (see Fig. 2) then translates to a difference in acidity of 5.5 pK_a units, which is reasonable.